European Journal of Computational Mechanics, 2014
Vol. 23, Nos. 5–6, 217–234, http://dx.doi.org/10.1080/17797179.2014.994964

Taylor & Francis
Taylor & Francis Group

Fracture with nonlocal elasticity: analytical and meshless approaches

P.H. Wen[a]*, X.J. Huang[a] and M.H. Aliabadi[b]

[a]*School of Engineering and Material Sciences, Queen Mary, University of London, London E1 4NS, UK;* [b]*Department of Aeronautics, Imperial College, London SW7 2BY, UK*

In this paper, two-dimensional fracture mechanics problem using the theory of nonlocal elasticity is investigated. According to the Eringen's model, the nonlocal stresses at the crack tip are regular. Based on the nonlocal theory, the stresses at the crack tip are approximated using the singular stress fields of the classical elasticity theory. A closed form approximate estimation of stresses at the crack tip is proposed using the stress intensity factors of the classical theory. The mesh reduction formulation of Local Integral Equation Method (LIEM) is also developed for the nonlocal theory to allow for numerical solution of 2D fracture problems. A central crack in a rectangular plate subjected to tensile load is solved using the proposed approach.

Keywords: Nonlocal elasticity, fracture mechanics, Eringen's model, meshless method of weak form

1. Introduction

The fundamental postulate of linear elastic fracture mechanics is that the behaviour of cracks is determined by the stress intensity factor. The stress intensity factor represents the strength of the stress singularity at the tip of a crack (Irwin, 1957). This assumption has followed the pioneering experimental observations of Griffith on the strength of different glass rods. Ever since, fracture mechanics problems and in particular crack-tip problems have been the subject of numerous publications, and many different methods have been developed for the evaluation of stress intensity factors for both static and dynamics loadings (Aliabadi, Rooke, & Cartwright, 1987; Dirgantara & Aliabadi, 2000; Fedelinski, Aliabadi, & Rooke, 1996; Rooke, Rayaprolu, & Aliabad, 1992; Wen, Aliabadi, & Rooke, 1998). It is well known that the classical continuum theories such as the linear theory of elasticity are intrinsically size independent. According to the classical theories, the elastic strains and stresses are singular at the crack tip. The continuum damage mechanics has been established to fill the gap between the classical continuum mechanics and fracture mechanics (see for e.g. (Bazant, 1976; Sfantos & Aliabadi, 2007)). A continuum model for microcracking in these materials leads inevitably to strain softening. It causes a loss of positive definiteness of the elastic modulus matrix and results as an ill-posed boundary value problem (Bazant & Lin, 1988; Benedetti & Aliabadi, 2013). The finite elements calculations using elasto-plastic models with yield limit degradation in the framework of the classical theory of plasticity give very different results for different meshes (Bazant, Belytschko, & Chang, 1984). In other words, the finite elements results are not independent with respect to the mesh refinements and converge at infinite mesh refinement to a solution with zero

*Corresponding author. Email: p.h.wen@qmul.ac.uk

energy dissipation during failure. To prevent such physically unrealistic behaviour, the mathematical models with localisation limits that force the strain-softening region to have a certain minimum finite size have been proposed in Sladek, Sladek, and Bazant (2003). A nonlocal elastic model proposed by Erigen (1983, 2002) and reviewed by Altan (1989) is based on the key idea that the long-range forces are adequately described by a constitutive relation. A theory of nonlocal elasticity of bi-Helmholtz type is suited based on the Erigen's model by Lazar, Maugin, and Aifantis (2006). The nonlocal finite element method (NL-FEM) was developed by Pisano, Sofi, and Fuschi (2009) based on the Eringen-type nonlocal elastic model with a constitutive stress–strain law of convolutive type which governs the nonlocal material behaviour. Mallardo (2009) presented the integral equation approach developed to describe elastic-damaging materials with an isotropic damage model implemented to study nonlinear structural problems involving localisation phenomena.

In recent years, the computational mechanics community has turned its attention to the so-called mesh reduction methods. These mesh reduction methods (commonly referred to as Meshless or Mesh free) have received much interest (Atluri, 2004; Li, Wen, & Aliabadi, 2011; Sladek & Sladek, 2006; Sladek, Sladek, & Zhang, 2006; Wen & Aliabadi, 2008; Wen, Aliabadi, & Liu, 2008). One key feature of these methods is that meshless methods do not need any grid and are, hence, meshless. More recently, a family of meshless methods based on the local weak Petrov-Galerkin formulation (MLPGs) for arbitrary partial differential equations with moving least square (MLS) approximation has been developed (Atluri, 2004). MLPG is reported to provide a rational basis for constructing meshless methods with a greater degree of flexibility. Local boundary integral equation method (LBIE) with moving least square and polynomial radial basis function (RBF) has been developed by Sladek et al. (2006). Both methods (MLPG and LBIE) are meshless, as no domain/boundary meshes are required in these two approaches. However, Galerkin-base meshless methods, except MLGP presented by Atluri (Mallardo, 2009) still include several awkward implementation features such as numerical integrations in the local domain. Other recent developments can be found in Sladek and Sladek (2006).

In this paper, application of the nonlocal elasticity theory to fracture mechanics is investigated. The stresses at the crack tip are shown to be regular and estimated using the mixed-mode stress intensity factors of the classical theory. Two-dimensional local boundary integral method (LIEM) is developed for the nonlocal elasticity theory with 2D Eringen's model. The numerical procedure is demonstrated for a rectangular plate with a central crack subjected to tensile load.

2. Analytical estimation of stress fields near crack tip

The nonlocal elastic model (Eringen, 1983, 2002) is based on the key idea that they are adequately described by a constitutive relation of the form (for two-dimension isotropic medium):

$$\sigma_{ij,j}(\mathbf{x}) + f_i(\mathbf{x}) = 0$$

$$\boldsymbol{\sigma}(\mathbf{x}) = \xi_1 \bar{\boldsymbol{\sigma}}(\mathbf{x}) + \xi_2 \int_V \alpha(\mathbf{x}, \mathbf{x}', l)\mathbf{D}\boldsymbol{\varepsilon}(\mathbf{x}')dV(\mathbf{x}') \tag{1}$$

$$\boldsymbol{\sigma} = \{\sigma_{11}, \sigma_{22}, \sigma_{12}\}^T, \quad \boldsymbol{\varepsilon} = \{\varepsilon_{11}, \varepsilon_{22}, \varepsilon_{12}\}^T, \quad \bar{\boldsymbol{\sigma}} = \mathbf{D}\boldsymbol{\varepsilon}, \quad \varepsilon_{ij} = (u_{i,j} + u_{j,i})/2$$

where ξ_1 and ξ_2 are sub-sections and $\xi_1 + \xi_2 = 1$, V represents the volume of domain, f_i body forces, α a nonlocal kernel defined as the influence coefficient, l the characteristic length or influence distance; $\mathbf{x}(x,y)$, $\mathbf{x}'(x',y')$ are collocation and domain integration points and u_i displacements; $\boldsymbol{\sigma}$, $\bar{\boldsymbol{\sigma}}$ and $\boldsymbol{\varepsilon}$ are vectors of nonlocal stress, local stress (classical stress) and strain; $\mathbf{D}$ denotes the elastic modulus matrix. The nonlocal kernel $\alpha(\mathbf{x}, \mathbf{x}', l) = \alpha(|\mathbf{x} - \mathbf{x}'|/l) = \alpha(r/l)$ has to satisfy the normalisation condition as

$$\int_{V_\infty} \alpha(|\mathbf{x} - \mathbf{x}'|/l) dV' = 1 \tag{2}$$

in which V_∞ indicates the infinite domain embedding V. For two-dimensional problem, one option of nonlocal kernels (type A) is $\alpha_A(\mathbf{x}, \mathbf{x}', l) = K_0(|\mathbf{x} - \mathbf{x}'|/l)/2\pi l^2$, where K_0 is the modified Bessel function of the first kind. For analytical estimation, a particular case of $\xi_1 = 0$ is considered. For an infinite plate with a straight line crack, the local displacement and stress fields in the domain are proved to be the same as elasticity (Eringen, 1983), that is,

$$\boldsymbol{\sigma}(\mathbf{x}) = \int_V \alpha_A(\mathbf{x}, \mathbf{x}', l) \bar{\boldsymbol{\sigma}}(\mathbf{x}') dV(\mathbf{x}') \tag{3}$$

where $\bar{\boldsymbol{\sigma}}(\mathbf{x})$ is classical local stress solution under the same boundary condition. Because of the displacement fields of the classical elastostatics are exactly the same as the nonlocal elastostatics (Bazant et al., 1984), we can borrow the displacement field from the well-known classical solution. It follows that the constitutive equations of the nonlocal theory give the stress field, as

$$\bar{\boldsymbol{\sigma}}(\mathbf{x}) = \boldsymbol{\sigma}_c(\mathbf{x}) \tag{4}$$

where $\boldsymbol{\sigma}_c(\mathbf{x})$ indicates the stress tensor of classical theory under the same boundary condition. Firstly, we consider a uniform tensile load σ_0 at infinite and the elasticity solution at point $\mathbf{x}' = (x', y')$ is given, in complex variable as

$$\begin{aligned} \bar{\sigma}_{22}(\mathbf{x}') + \bar{\sigma}_{11}(\mathbf{x}') &= \sigma_0 \mathrm{Re}\left(\frac{2z'}{\sqrt{z'^2 - a^2}} - 1\right) \\ \bar{\sigma}_{22}(\mathbf{x}') - \bar{\sigma}_{11}(\mathbf{x}') + 2i\bar{\sigma}_{12}(\mathbf{x}') &= \sigma_0 \left(\frac{2ia^2 y'}{\sqrt{(z'^2 - a^2)^3}} + 1\right) \end{aligned} \tag{5}$$

where a is half-length crack, complex variable $z' = x' + iy'$ and $i = \sqrt{-1}$. Therefore, the solution of nonlocal elasticity becomes

$$\begin{aligned} \sigma_{22}(\mathbf{x}) = \frac{\sigma_0}{2\pi l^2} \int_0^\infty \int_0^{2\pi} \mathrm{Re}\left(\frac{z'}{\sqrt{z'^2 - a^2}} + \frac{ia^2 y'}{\sqrt{(z'^2 - a^2)^3}}\right) K_0(|\mathbf{x} - \mathbf{x}'|/l) r d\theta dr \\ \mathbf{x}' = (a + r\cos\theta, r\sin\theta), \quad z' = a + re^{i\theta}. \end{aligned} \tag{6}$$

Moreover, the nonlocal elasticity solution of stress σ_{22} along axis x is obtained

$$\sigma_{22}(x, 0) = \frac{\sigma_0}{2\pi l^2} \int_0^\infty \int_0^{2\pi} \mathrm{Re}\left(\frac{z'}{\sqrt{z'^2 - a^2}} + \frac{ia^2 y'}{\sqrt{(z'^2 - a^2)^3}}\right) K_0(R/l) r d\theta dr \tag{7}$$

where $R=\sqrt{(a+r\cos\theta-x)^2+r^2\sin^2\theta}$. Considering only the singular stress field, an approximate solution can be obtained from the classical local elasticity (Irwin, 1957) in the vicinity of the crack tip as

$$\bar{\sigma}_{22}(r,\theta)=\frac{K_I}{\sqrt{2\pi r}}\cos\frac{\theta}{2}\left(1+\sin\frac{\theta}{2}\cos\frac{3\theta}{2}\right) \tag{8}$$

Hence, estimation of nonlocal stress distribution is obtained as

$$\sigma^*_{22}(x,0)=\frac{\sigma_0\sqrt{a}}{2\pi l^2\sqrt{2}}\int_0^{\infty}\int_0^{2\pi}\cos\frac{\theta}{2}\left(1+\sin\frac{\theta}{2}\cos\frac{3\theta}{2}\right)K_0(R/l)\sqrt{r}d\theta dr \tag{9}$$

The variation of normalised stresses $\sigma_{22}(x,0)/\sigma_0$ and $\sigma^*_{22}(x,0)/\sigma_0$ along axis $x(=a+\xi)$ is shown in Figures 1(a), (b) and (c) for different ratios l/a. It is apparent that the stress distribution for nonlocal theory is regular along axis x including the crack tip. At the crack tip, from (7), we have the stress distribution exactly

$$\sigma_{22}(a,0)=\frac{\sigma_0}{2\pi l^2}\int_0^{\infty}\int_0^{2\pi}\mathrm{Re}\left(\frac{a+re^{i\theta}}{\sqrt{2a+re^{i\theta}}}e^{-i\theta/2}+\frac{ia^2\sin\theta}{\sqrt{(2a+re^{i\theta})^3}}e^{-3i\theta/2}\right)K_0(r/l)\sqrt{r}d\theta dr. \tag{10}$$

Consider the singular stress field of the classical theory, approximated stress at the crack tip is obtained, from (9), as

$$\sigma^*_{22}(a,0)=\frac{K_I}{2\pi\sqrt{\pi l}}\int_0^{\infty}K_0(\lambda)\sqrt{\lambda}d\lambda=0.5736\sigma_0/\sqrt{\kappa} \tag{11}$$

where $K_I=\sigma_0\sqrt{\pi a}$ denotes the stress intensity factor for a central crack under uniform tensile at infinite and $\kappa=l/a$. In (Eringen, 1983), the factor is given as $0.5744\sigma_0/\sqrt{\kappa}$ by integral equation method, which is very close to the solution in (11). Figure 2 shows the variation of the normalised stress $\sigma_{22}(a,0)/[\sigma_0/\sqrt{\kappa}]$ at crack tip against the ratio l/a. The exact results from (10) can be presented approximately as

$$\sigma_{22}(a,0)=\frac{0.574\sigma_0}{\sqrt{\kappa}}(1+0.4315\kappa) \tag{12}$$

It is clear that the relative error of approximation solution in (11) is 0.4315κ. For example, when $\kappa=l/a=0.05$, the relative error of estimation is about 2%.

Secondly, consider a uniform shear stress τ_0 at infinite, the elasticity solution is given in

$$\begin{aligned}\bar{\sigma}_{22}(\mathbf{x}')+\bar{\sigma}_{11}(\mathbf{x}')&=-2\tau_0\mathrm{Re}\left(\frac{iz'}{\sqrt{z'^2-a^2}}\right)\\ \bar{\sigma}_{22}(\mathbf{x}')-\bar{\sigma}_{11}(\mathbf{x}')+2i\bar{\sigma}_{12}(\mathbf{x}')&=i\tau_0\frac{a^2\bar{z}'+z'(2z'^2-3a^2)}{\sqrt{(z'^2-a^2)^3}}.\end{aligned} \tag{13}$$

where $\bar{z}'=x'-iy'$. Thus, the distribution of shear stress along x axis is obtained

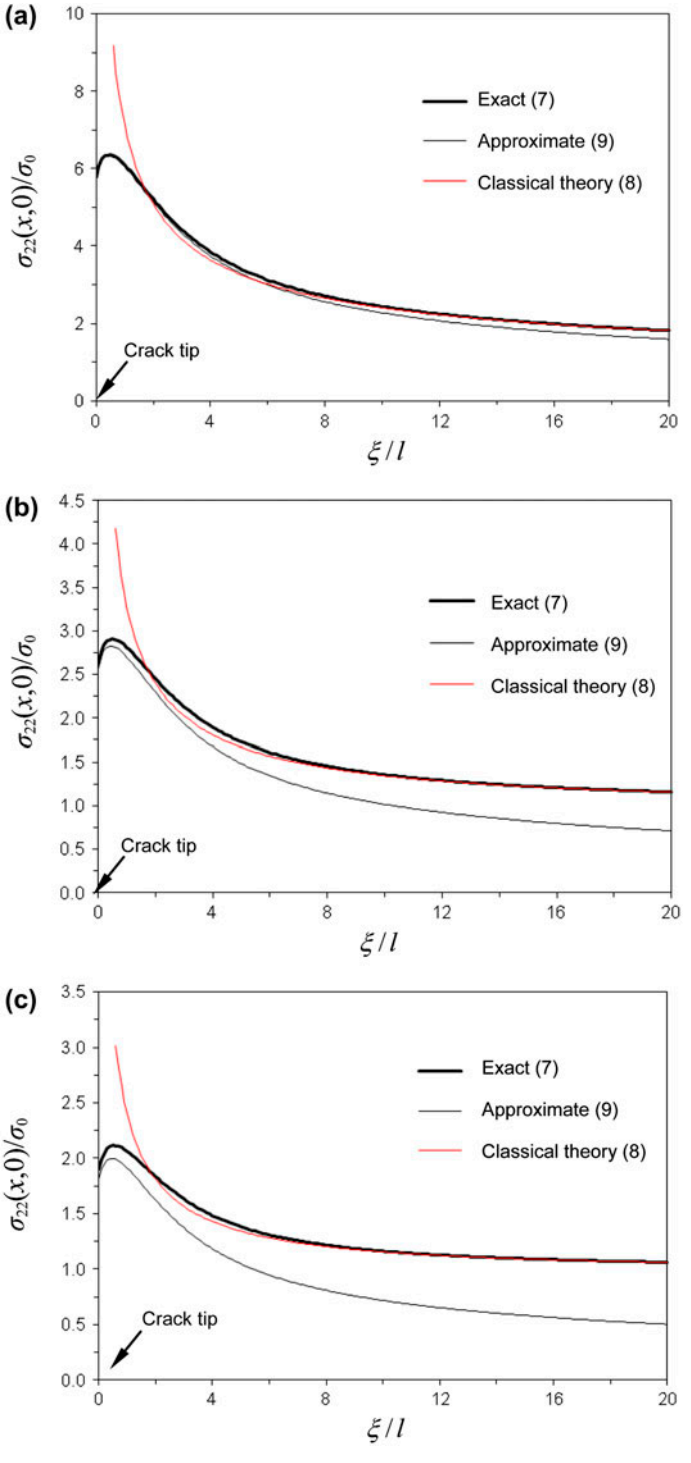

Figure 1. Normalised stress $\sigma_{22}(x,0)/\sigma_0$ verse x $(=a+\xi)$: (a) $l/a = 0.01$; (b) $l/a = 0.05$; (c) $l/a = 0.1$.

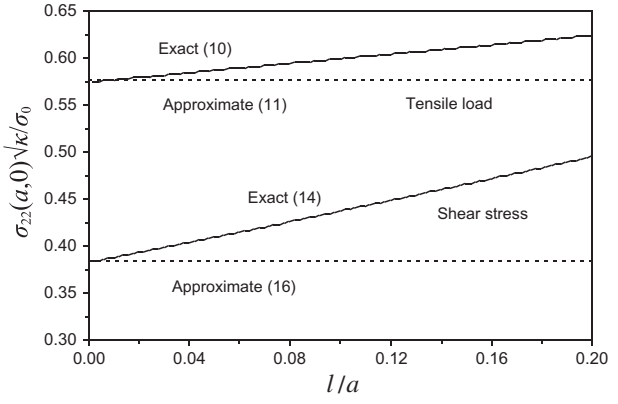

Figure 2. Comparison of normalised stresses $\sqrt{\kappa}\sigma_{22}(a,0)/\sigma_0$ and $\sqrt{\kappa}\sigma_{12}(a,0)/\tau_0$ at the crack tip with exact and approximate solutions.

$$\sigma_{12}(x,0) = \tfrac{\tau_0}{4\pi l^2}\int_0^\infty\int_0^{2\pi} \mathrm{Re}\left(\frac{a^2\bar{z}' + z'(2z'^2 - 3a^2)}{\sqrt{(z'^2 - a^2)^3}}\right) K_0(R/l) r d\theta dr \tag{14}$$
$$R = \sqrt{(a + r\cos\theta - x)^2 + r^2\sin^2\theta}$$

For a small ratio of r/a, one has the classical elastic stress as (Irwin, 1957)

$$\bar{\sigma}_{12}(r,\theta) = \frac{K_{II}}{\sqrt{2\pi r}}\cos\frac{\theta}{2}\left(1 - \sin\frac{\theta}{2}\cos\frac{3\theta}{2}\right) \tag{15}$$

and then the estimated nonlocal shear stress at the crack tip is

$$\sigma^*_{12}(a,0) = \frac{K_{II}}{2\pi\sqrt{\pi l}}\int_0^\infty K_0(\lambda)\sqrt{\lambda}d\lambda = 0.3824\tau_0/\sqrt{\kappa} \tag{16}$$

where $K_{II} = \tau_0\sqrt{\pi a}$ denotes the shear mode stress intensity factor. In addition, the exact nonlocal shear stress at the crack tip from (14) is shown in Figure 2 and can be written approximately as

$$\sigma_{12}(a,0) = \frac{0.3812\tau_0}{\sqrt{\kappa}}(1 + 1.4743\kappa) \tag{17}$$

Same as the tensile stress, the relative error of approximation solution for shear loading in (16) is 1.4743κ. To determine the stress at the crack tip, we can extend this computation procedure for a finite cracked plate. For mixed-mode crack problems, in general cases, if the stress intensity factors of the classical theory are denoted as K_I and K_{II}, respectively, the nonlocal stresses at the crack tip are regular and can be estimated from (11) and (16) for a small ratio of $l/a(<0.05)$, as

$$\sigma^*_{22}(a,0) = 0.5736K_I/\sqrt{\pi l}, \quad \sigma^*_{12}(a,0) = 0.3824K_{II}/\sqrt{\pi l}. \tag{18}$$

Obviously, the degree of accuracy depends on the ratio κ and the dimension of geometry of cracked plate, which can be seen from Figure 2. In addition, maximum normal and shear stresses exist at $\xi/l = 0.5$ and they are given by Eringen (1983) approximately, for a small ratio of κ, as

$$\sigma_{22,\max}(a+\xi,0) = 1.12\sigma_{22}(a,0). \tag{19}$$

Next, more nonlocal kernels (Type) are observed. Select the following coefficient functions as

$$\alpha_B(r,l) = \frac{1}{2\pi l^2} e^{-r/l}$$

$$\alpha_C(r,l) = \frac{1}{\pi l^2} e^{-r^2/l^2}$$

$$\alpha_D(r,l) = \begin{cases} \frac{3}{\pi l^2}\left(1-\frac{r}{l}\right) & r \le l \\ 0 & r \ge l \end{cases} \tag{20}$$

$$\alpha_E(r,l) = \begin{cases} \frac{2}{\pi l^2}\left(1-\frac{r^2}{l^2}\right) & r \le l \\ 0 & r \ge l \end{cases}$$

where $r = |\mathbf{x} - \mathbf{x}'|$. From (3), (8) and (15), for Type B, one has the estimation of stress at the crack tip

$$\begin{aligned} \sigma_{22}^*(a,0) &= \tfrac{6\sqrt{2}K_I}{5\pi\sqrt{\pi l}} \int_0^\infty \sqrt{t} e^{-t} dt = 0.4787 \tfrac{K_I}{\sqrt{\pi l}} \\ \sigma_{12}^*(a,0) &= \tfrac{4\sqrt{2}K_{II}}{5\pi\sqrt{\pi l}} \int_0^\infty \sqrt{t} e^{-t} dt = 0.3192 \tfrac{K_{II}}{\sqrt{\pi l}} \end{aligned} \tag{21}$$

and for Type C,

$$\begin{aligned} \sigma_{22}^*(a,0) &= \frac{3\sqrt{2}K_I}{5\pi\sqrt{\pi l}} \int_0^\infty \sqrt{t} e^{-t^2} dt = 0.6620 \frac{K_I}{\sqrt{\pi l}} \\ \sigma_{12}^*(a,0) &= \frac{2\sqrt{2}K_{II}}{5\pi\sqrt{\pi l}} \int_0^\infty \sqrt{t} e^{-t^2} dt = 0.4413 \frac{K_{II}}{\sqrt{\pi l}}. \end{aligned} \tag{22}$$

It is not difficult to obtain the normal and shear stresses at the crack tip for the rest of coefficient functions. Normalised stresses $\sigma_{22}^*\sqrt{\pi l}/K_I$ and $\sigma_{12}^*\sqrt{\pi l}/K_{II}$ are presented in Table 1 for different types. Moreover, for Type C, the shear stress at the crack tip by Erigen (1983) is derived to be $0.4243\tau_0/\sqrt{\kappa}$. Compared with these two solutions (0.4243 and 0.4413), the relative error is less than 4%. However, the estimation in this paper should be more accurate for a small ratio of l/a. Tables 2 and 3 show the exact maximum nonlocal stresses and their locations when $l/a = 0.01$ from (7) and (14) for different nonlocal kernels (Type).

Table 1. Nonlocal stresses at crack tip for different Types.

Type	A	B	C	D	E
$\sigma_{22}^*\sqrt{\pi l}/K_I$	0.5736	0.4787	0.6620	0.8643	0.8231
$\sigma_{12}^*\sqrt{\pi l}/K_{II}$	0.3824	0.3192	0.4413	0.5762	0.5488

Table 2. Maximum nonlocal normal stress $\sigma_{22,\max}(a+\xi,0)/\sigma_{22}(a,0)$ when $l/a = 0.01$.

Type	A	B	C	D	E
ξ/l	0.45	0.85	0.61	0.40	0.47
$\sigma_{22,\max}/\sigma_{22}(a,0)$	1.1029	1.1378	1.1830	1.1838	1.1947

Table 3. Maximum nonlocal shear stress $\sigma_{12,\max}(a+\xi,0)/\sigma_{12}(a,0)$ when $l/a = 0.01$.

Type	A	B	C	D	E
ξ/l	0.55	1.30	0.88	0.54	0.65
$\sigma_{12,\max}/\sigma_{12}(a,0)$	1.0898	1.1203	1.1548	1.1553	1.1742

3. Meshless method for nonlocal elasticity

It is too difficult to obtain analytical solution for the partial differential equation in (1) even for one-dimensional problem (Li et al., 2013). Pisano et al. (2009) applied the finite element analysis to nonlocal elasticity. In this section, one meshless method, named the local integral equation method (Wen & Aliabadi, 2013) is applied to deal with nonlocal elasticity. In this numerical analysis procedure, subscripts are used to indicate the coordinate system. Two kinds of boundary conditions are considered for nonlocal elasticity, namely, for nonlocal traction boundary

$$\sigma_{ij}n_j = t_i^0 \tag{23}$$

and for displacement boundary

$$u_i = u_i^0 \tag{24}$$

in which u_i^0 and t_i^0 are the prescribed displacements and tractions, respectively, on the displacement boundary Γ_D and on the traction boundary Γ_T, and n_i is the unit normal outward to the boundary Γ.

In the nonlocal integral equation approach, the weak form of differential equation over a local integral domain Ω_s can be written, from (1), as

$$\int_{\Omega_s} \left[\sigma_{ij,\,j}(\mathbf{x}) + f(\mathbf{x})\right] u_i^*(\mathbf{x}) d\Omega(\mathbf{x}) = 0 \tag{25}$$

where $u_i^*(\mathbf{x})$ is the test function. By use of the divergence theorem, (25) above can be rewritten in a symmetric weak form as

$$\int_{\Gamma_s} \sigma_{ij}n_j u_i^* d\Gamma - \int_{\Omega_s} (\sigma_{ij}u_{i,\,j}^* - f_i u_i^*) d\Omega = 0. \tag{26}$$

If there is an intersection between the local boundary and the global boundary, a local symmetric weak form in linear elasticity may be written as

$$\int_{\Omega_s} \sigma_{ij}u_{i,\,j}^* d\Omega - \int_{L_s} t_i u_i^* d\Gamma - \int_{\Gamma_D} t_i u_i^* d\Gamma = \int_{\Gamma_T} t_i^0 u_i^* d\Gamma + \int_{\Omega_s} f_i u_i^* d\Omega \tag{27}$$

in which L_s indicates the other part of the local boundary inside the local integral domain Ω_s; Γ_D is the intersection between the local boundary Γ_s and the global displacement boundary; and Γ_T is a part of the traction boundary as shown in Figure 3.

The weak forms in (26) and (27) are a starting point to derive local boundary integral equations if appropriate test functions are selected. Step functions can be used as the test functions u_i^* in each integral domain

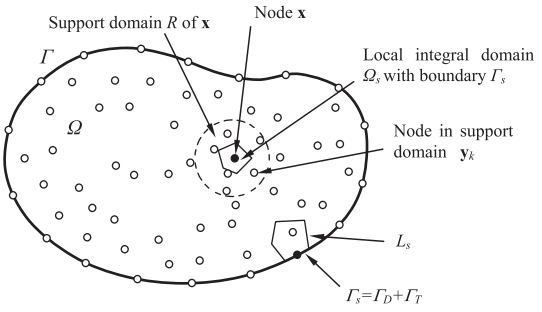

Figure 3. Arbitrary distributed node, support domain of **x**, local integral domain for weak formulation.

$$u_i^*(\mathbf{x}) = \begin{cases} \varphi_i(\mathbf{x}) & \text{at } \mathbf{x} \in (\Omega_s \cup \Gamma_s) \\ 0 & \text{at } \mathbf{x} \notin \Omega_s \end{cases} \tag{28}$$

where $\varphi_i(\mathbf{x})$ is an arbitrary function. For $\varphi_i(\mathbf{x}) = 1$ and zero body force $f_i = 0$, the weak forms (26) and (27) are transformed into simple local boundary integral equations (equilibrium of local integral domain) as

$$\int_{\Gamma_s} t_i d\Gamma = 0 \tag{29}$$

and

$$\int_{L_s+\Gamma_D} t_i d\Gamma = -\int_{\Gamma_T} t_i^0 d\Gamma. \tag{30}$$

Consider a local domain $\partial\Omega_s$ shown in Figure 3, which is the neighbourhood of a point $\mathbf{x}[=(x_1, x_2)]$ and is considered as the domain of definition of the RBF approximation for the trail function at **x** and also called the support domain to an arbitrary point **x**. Generally, the support domain is chosen as a circle R centred at **x,** as shown in Figure 3. To interpolate the distribution of function u in the local domain $\partial\Omega_s$ over a number of randomly distributed nodes, i.e. $\{\mathbf{y}_1, \mathbf{y}_2, \ldots, \mathbf{y}_K\}$, $\mathbf{y}_k\left[=\left(y_1^k, y_2^k\right)\right]$, $k = 1, 2, \ldots, K$, the approximation of function u at the point **x** can be expressed by

$$u_i(\mathbf{x}) = \sum_{k=1}^{K} R_k(\mathbf{x}, \mathbf{y}_k)\alpha_k + \sum_{t=1}^{T} P_t(\mathbf{x})\beta_t = \mathbf{R}(\mathbf{x})\alpha + \mathbf{P}(\mathbf{x})\boldsymbol{\beta} \tag{31}$$

where $\mathbf{R}(\mathbf{x}) = \{R_1(\mathbf{x}, \mathbf{y}_1), R_2(\mathbf{x}, \mathbf{y}_2), \ldots, R_K(\mathbf{x}, \mathbf{y}_K)\}$ is set of radial basis functions centred around the point **x**, $\{\alpha_k\}_{k=1}^{K}$ and $\{\beta_t\}_{t=1}^{T}$ are unknowns to be determined and $\{P_t\}_{t=1}^{T}$ is a basis for P_{T-1}, the set of d-variate polynomials of degree $\leq T-1$. The radial basis function selected multiquadrics as

$$R_k(\mathbf{x}, \mathbf{y}_k) = \sqrt{c^2 + \left[x_1 - y_1^k\right]^2 + \left[x_2 - y_2^k\right]^2} \tag{32}$$

where c is a free parameter and along with the constraints

$$\sum_{k=1}^{K} P_t(\mathbf{y}_k)\alpha_k = 0, \qquad 1 \le t \le T \tag{33}$$

In this paper, the following polynomials are considered if $T = 6$

$$\mathbf{P} = \left\{1, x_1, x_2, x_1^2, x_1x_2, x_2^2\right\} \tag{34}$$

A set of linear equations can be written in the matrix form as

$$\mathbf{R}_0\boldsymbol{\alpha} + \mathbf{P}\boldsymbol{\beta} = \hat{\mathbf{u}}, \qquad \mathbf{P}^T\boldsymbol{\alpha} = \mathbf{0} \tag{35}$$

where $\hat{\mathbf{u}}$ is the vector containing all the field nodal values at the L local nodes and the coefficient matrices are defined as

$$\begin{aligned}
\mathbf{R}_0 &= \begin{bmatrix} R_1(\mathbf{y}_1,\mathbf{y}_1) & R_2(\mathbf{y}_1,\mathbf{y}_2) & \dots & R_K(\mathbf{y}_1,\mathbf{y}_K) \\ R_1(\mathbf{y}_2,\mathbf{y}_1) & R_2(\mathbf{y}_2,\mathbf{y}_2) & \dots & R_K(\mathbf{y}_2,\mathbf{y}_K) \\ \cdot & \cdot & \cdots & \cdot \\ \cdot & \cdot & \cdots & \cdot \\ \cdot & \cdot & \cdots & \cdot \\ R_1(\mathbf{y}_N,\mathbf{y}_1) & R_2(\mathbf{y}_N,\mathbf{y}_2) & \dots & R_K(\mathbf{y}_K,\mathbf{y}_K) \end{bmatrix}, \\
\mathbf{P} &= \begin{bmatrix} P_1(\mathbf{y}_1) & P_2(\mathbf{y}_1) & \dots & P_T(\mathbf{y}_1) \\ P_1(\mathbf{y}_2) & P_2(\mathbf{y}_2) & \dots & P_T(\mathbf{y}_2) \\ \cdot & \cdot & \cdots & \cdot \\ \cdot & \cdot & \cdots & \cdot \\ \cdot & \cdot & \cdots & \cdot \\ P_1(\mathbf{y}_K) & P_2(\mathbf{y}_K) & \dots & P_T(\mathbf{y}_K) \end{bmatrix}
\end{aligned} \tag{36}$$

Solving equation (35) gives

$$\boldsymbol{\beta} = \left(\mathbf{P}^{\mathrm{T}}\mathbf{R}_0^{-1}\mathbf{P}\right)^{-1}\mathbf{P}^{\mathrm{T}}\mathbf{R}_0^{-1}\hat{\mathbf{u}}, \qquad \boldsymbol{\alpha} = \mathbf{R}_0^{-1}\left[\mathbf{I} - \mathbf{P}\left(\mathbf{P}^{\mathrm{T}}\mathbf{R}_0^{-1}\mathbf{P}\right)^{-1}\mathbf{P}^{\mathrm{T}}\mathbf{R}_0^{-1}\right]\hat{\mathbf{u}} \tag{37}$$

where $\mathbf{I}$ denotes the diagonal unit matrix. Substituting the coefficients $\boldsymbol{\alpha}$ and $\boldsymbol{\beta}$ from (37) into (31), we can obtain the approximation of the field function, in terms of the nodal values

$$\begin{aligned}
u(\mathbf{x}) &= \left\langle \mathbf{R}(\mathbf{x})\mathbf{R}_0^{-1}\left[\mathbf{I} - \mathbf{P}\left(\mathbf{P}^{\mathrm{T}}\mathbf{R}_0^{-1}\mathbf{P}\right)^{-1}\mathbf{P}^{\mathrm{T}}\mathbf{R}_0^{-1}\right] + \mathbf{P}(\mathbf{x})\left(\mathbf{P}^{\mathrm{T}}\mathbf{R}_0^{-1}\mathbf{P}\right)^{-1}\mathbf{P}^{\mathrm{T}}\mathbf{R}_0^{-1}\right\rangle\hat{\mathbf{u}} \\
&= \sum_{i=1}^{K}\phi_i(\mathbf{x})\hat{u}_i = \boldsymbol{\Phi}(\mathbf{x})\hat{\mathbf{u}}
\end{aligned} \tag{38}$$

where $\Phi(\mathbf{x}) = \{\phi_1(\mathbf{x}), \phi_2(\mathbf{x}), \ldots, \phi_K(\mathbf{x})\}$ is called as shape function. It is worth noticing that the shape function depends uniquely on the distribution of scattered nodes within the domain and has the Kronecker delta property.

Consider a unit test function, i.e. $\varphi_i(\mathbf{x}) = 1$, and the local domain is a circle shown in Figure 3; therefore, the local integral equation (26) becomes

$$\int_{\Gamma_s}\sigma_{ij}(\mathbf{x})n_j(\mathbf{x})d\Gamma(\mathbf{x}) = \xi_1\sum_{l=1}^{L}\bar{\sigma}_{ij}(\mathbf{x}_l)n_j^l\Delta_l + \xi_2\sum_{l=1}^{L}n_j^l\Delta_l\int_V\alpha(\mathbf{x}_l,\mathbf{x}',l)\bar{\sigma}_{ij}(\mathbf{x}')dV(\mathbf{x}') \tag{39}$$

where L is number of segment on the boundary of local integral domain, n_j^l and Δ_l are components of normal and length of segment l. Suppose there are M nodes both in the domain and on the boundary, $M = M_\Omega + M_T + M_D$, where M_Ω indicates the number of nodes collocated in the domain and M_T and M_D are numbers of nodes on the traction/

displacement boundaries and consider the relationship between stress and strain in (1), for the plane stress, (39) becomes

$$\begin{aligned}
&\xi_1 \sum_{k=1}^{K}\sum_{l=1}^{L}\Big[\big(E\phi_{k,1}(\mathbf{x})n_1^l/(1-v^2)+\mu\phi_{k,2}(\mathbf{x})n_2^l\big)u_1^{(k)} \\
&\qquad +\big(vE\phi_{k,2}(\mathbf{x})n_1^l/(1-v^2)+\mu\phi_{k,1}(\mathbf{x})n_2^l\big)u_2^{(k)}\Big]\Delta_l \\
&+\xi_2 \sum_{k'=1}^{K'} u_1^{(k')}\int_V\left[\sum_{l=1}^{L}\big(E\phi_{k',1}(\mathbf{x}')n_1^l/(1-v^2)+\mu\phi_{k',2}(\mathbf{x}')n_2^l\big)\alpha(\mathbf{x}_l,\mathbf{x}',l)\Delta_l\right]dV(\mathbf{x}') \\
&+\xi_2 \sum_{k'=1}^{K'} u_2^{(k')}\int_V\left[\sum_{l=1}^{L}\big(vE\phi_{k',2}(\mathbf{x}')n_1^l/(1-v^2)+\mu\phi_{k',1}(\mathbf{x}')n_2^l\big)\alpha(\mathbf{x}_l,\mathbf{x}',l)\Delta_l\right]dV(\mathbf{x}') \\
&=0
\end{aligned} \tag{40a}$$

$$\begin{aligned}
&\xi_1 \sum_{k=1}^{K}\sum_{l=1}^{L}\Big[\big(vE\phi_{k,1}(\mathbf{x})n_2^l/(1-v^2)+\mu\phi_{k,2}(\mathbf{x})n_1^l\big)u_1^{(k)} \\
&\qquad +\big(E\phi_{k,2}(\mathbf{x})n_1^l/(1-v^2)+\mu\phi_{k,1}(\mathbf{x})n_2^l\big)u_2^{(k)}\Big]\Delta_l \\
&+\xi_2 \sum_{k'=1}^{K'} u_1^{(k')}\int_V\left[\sum_{l=1}^{L}\big(vE\phi_{k',1}(\mathbf{x}')n_2^l/(1-v^2)+\mu\phi_{k',2}(\mathbf{x}')n_1^l\big)\alpha(\mathbf{x}_l,\mathbf{x}',l)\Delta_l\right]dV(\mathbf{x}') \\
&+\xi_2 \sum_{k'=1}^{K'} u_2^{(k')}\int_V\left[\sum_{l=1}^{L}\big(\mu\phi_{k',1}(\mathbf{x}')n_2^l+E_k',2(\mathbf{x}')n_1^l/(1-v^2)\big)\alpha(\mathbf{x}_l,\mathbf{x}',l)\Delta_l\right]dV(\mathbf{x}') \\
&=0
\end{aligned} \tag{40b}$$

where $k'=1,2,\ldots K'$ are the numbers of node in the support domain centred $(\mathbf{x}')$ at the local integral area $dV(\mathbf{x}')$, E and μ are the Young's modulus and shear modulus, v is the Poisson's ratio. For all domain integrals, four-point standard integral scheme is adopted in computation. Then, (40a) and (40b) above are rewritten as

$$\begin{aligned}
&\xi_1 \sum_{k=1}^{K}\sum_{l=1}^{L}\Big[\big(E\phi_{k,1}(\mathbf{x})n_1^l/(1-v^2)+\mu\phi_{k,2}(\mathbf{x})n_2^l\big)u_1^{(k)} \\
&\qquad +\big(vE\phi_{k,2}(\mathbf{x})n_1^l/(1-v^2)+\mu\phi_{k,1}(\mathbf{x})n_2^l\big)u_2^{(k)}\Big]\Delta_l \\
&+\xi_2 \sum_{k'=1}^{K'} u_1^{(k')}\sum_{q=1}^{Q}\sum_{p=1}^{4}\sum_{l=1}^{L}\Big(E\phi_{k',1}(\mathbf{x}'_{qp})n_1^l/(1-v^2)+\mu\phi_{k',2}(\mathbf{x}'_{qp})n_2^l\Big)\alpha(\mathbf{x}_l,\mathbf{x}'_{qp},l)\Delta_l w_p\Delta V_q \\
&+\xi_2 \sum_{k'=1}^{K'} u_2^{(k')}\sum_{q=1}^{Q}\sum_{p=1}^{4}\sum_{l=1}^{L}\Big(vE\phi_{k',2}(\mathbf{x}'_{qp})n_1^l/(1-v^2)+\mu\phi_{k',1}(\mathbf{x}'_{qp})n_2^l\Big)\alpha(\mathbf{x}_l,\mathbf{x}'_{qp},l)\Delta_l w_p\Delta V_q \\
&=0
\end{aligned} \tag{41a}$$

$$\xi_1 \sum_{k=1}^{K}\sum_{l=1}^{L}\Big[\big(vE\phi_{k,1}(\mathbf{x})n_2^l/(1-v^2)+\mu\phi_{k,2}(\mathbf{x})n_1^l\big)u_1^{(k)} +\big(E\phi_{k,2}(\mathbf{x})n_1^l/(1-v^2)+\mu\phi_{k,1}(\mathbf{x})n_2^l\big)u_2^{(k)}\Big]\Delta_l + \xi_2\sum_{k'=1}^{K'}u_1^{(k')}\sum_{q=1}^{Q}\sum_{p=1}^{4}\sum_{l=1}^{L}\Big(vE\phi_{k',1}(\mathbf{x}'_{qp})n_2^l/(1-v^2)+\mu\phi_{k',2}(\mathbf{x}'_{qp})n_1^l\Big)\alpha(\mathbf{x}_l,\mathbf{x}'_{qp},l)\Delta_l w_p\Delta V_q + \xi_2\sum_{k'=1}^{K'}u_2^{(k')}\sum_{q=1}^{Q}\sum_{p=1}^{4}\sum_{l=1}^{L}\Big(\mu\phi_{k',1}(\mathbf{x}'_{qp})n_2^l+E\phi_{k',2}(\mathbf{x}'_{qp})n_1^l/(1-v^2)\Big)\alpha(\mathbf{x}_l,\mathbf{x}'_{qp},l)\Delta_l w_p\Delta V_q = 0 \tag{41b}$$

where Q in the summation above represents the number of total rectangular segments of whole integral domain using a background grid, $\mathbf{x}'_{qp}=\mathbf{x}'_q+\mathbf{x}'_p$. For the nodes on the traction boundary, (29) should be introduced

$$\int_{\Gamma-\Gamma_T} t_i d\Gamma = -\int_{\Gamma_T} t_i^0 d\Gamma \quad \text{for } \mathbf{x}_k \quad k=1,2,\ldots,M_T \tag{42}$$

For the displacement boundary nodes, we can introduce the displacement equation directly, i.e. $u_i(\mathbf{x}_k)=u_i^0,\ k=1,2,\ldots M_D$. Therefore, there are $2\times(M_\Omega+M_T+M_D)$ linear algebraic equations in total to determine the same number unknowns of displacements either in the domain or on the traction boundary.

4. Rectangular plate with central crack

A rectangular plate of width $2b$ and height $2\,h$ containing a central crack of length 2a subjected to tensile load on the top is shown in Figure 4(a). Investigation for the free parameter selections has been done by many authors and therefore, it is not necessary to discuss in this section. In the following analysis, to the authors experience, we

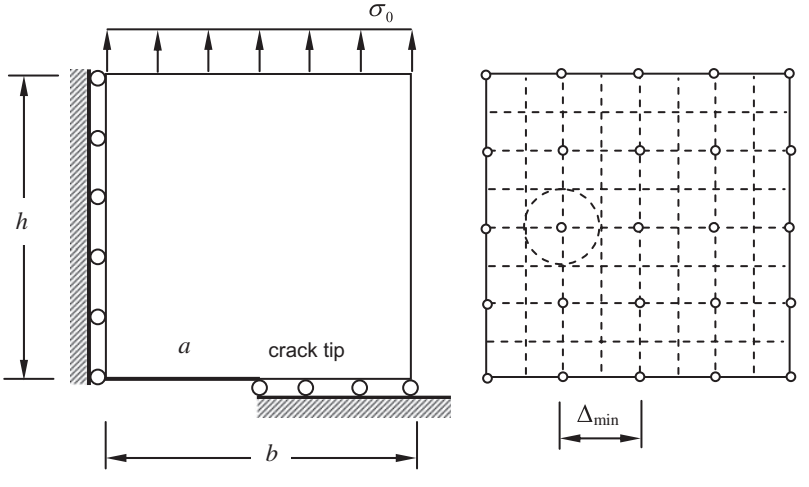

Figure 4. Rectangular plate with central crack: (a) quarter of plate and boundary conditions; (b) collocation point for local integral equation method and grid for domain integrals.

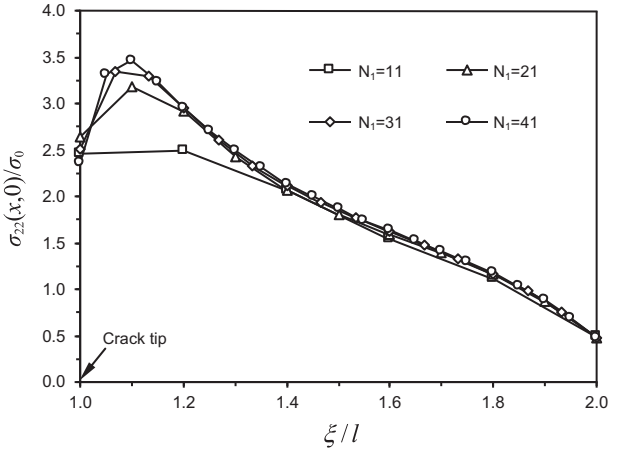

Figure 5. Distribution of normalised stress $\sigma_{22}(x,0)/\sigma_0$ for different densities of collocation point while $l/a = 0.1$ and $h = b = 2a$.

selected the free parameter in the radial bases function $c = \Delta_{\min}$ in (32), radius of local integral domain $R = \Delta_{\min}/2$ (Γ_s) and number of segment on local integral $L = 36$, $\Delta_{\min}$ indicates the minimum distance between the nodes in the local integral domain shown in Figure 4(b). The support domain is selected as a circle of radius r_0 centred at field point **x,** which is determined such that the minimum number of nodes in the support domain $K \geq N_0$, where the number N_0 is selected between 12 and 20. In addition, a grid of background for the domain integration as shown in Figure 4(b) is introduced to carry out all domain integrals in (41a) and (41b). The Poisson's ratio $v = 0.3$, the numbers of collocation points is $M(=N_1 \times N_2)$ and the number of integral sub-domain $Q(=V_1 \times V_2,\ V_i(=2(N_i - 1) + 1))$. As symmetry of the plate and load condition,

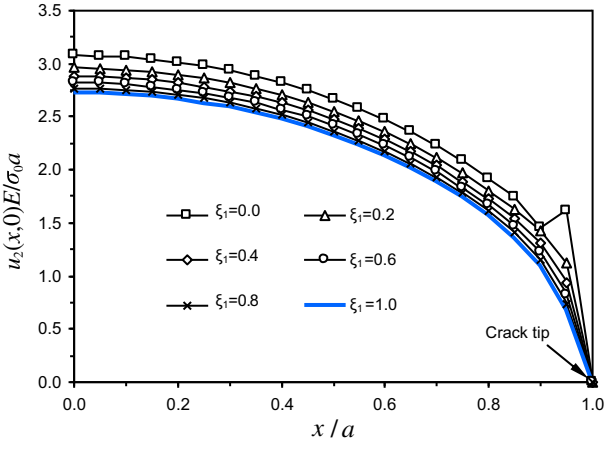

Figure 6. Opening displacement $u_2(x,0)E/\sigma_0 a$ for different portion of nonlocal elasticity while $l/a = 0.05$ and $h = b = 2a$.

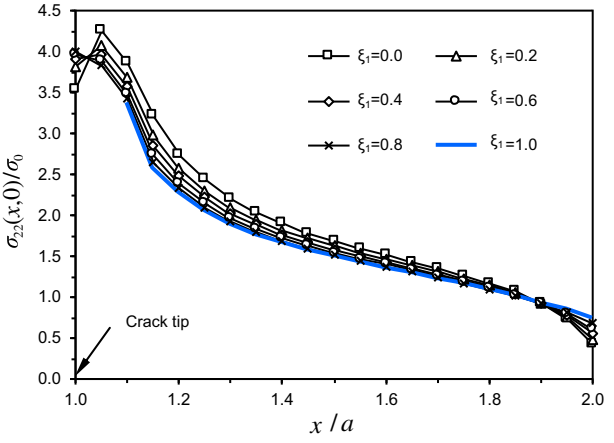

Figure 7. Normalised stress $\sigma_{22}(x,0)/\sigma_0$ for different portions of nonlocal elasticity while $l/a = 0.05$ and $h = b = 2a$.

quarter of plate is analysed. However, the integrals of whole domain for nonlocal elasticity must be taken into account.

First of all, the convergence of numerical method is observed. Figure 5 shows the distribution of the normalised stress for different densities of collocation point for the square plate $(b/a = h/a = 2)$ and ratio $l/a = 0.1$. Obviously, the maximum stress is located about $\xi/l = 0.5$, which agrees with the conclusion of the analytical approach.

Next, the displacement on the crack surface and stress are observed when $l/a = 0.05$. The variations of crack opening displacement $u_2 E/\sigma_0 a$ and the normalised stresses σ_{22}/σ_0 along x axis for different portion factor ξ_1 with geometry of plate $h = b = 2a$ are shown in Figure 6 and Figure 7, respectively. It can be found that the displacement is minimum for the case of classical elasticity $\xi_1 = 1$. However, the

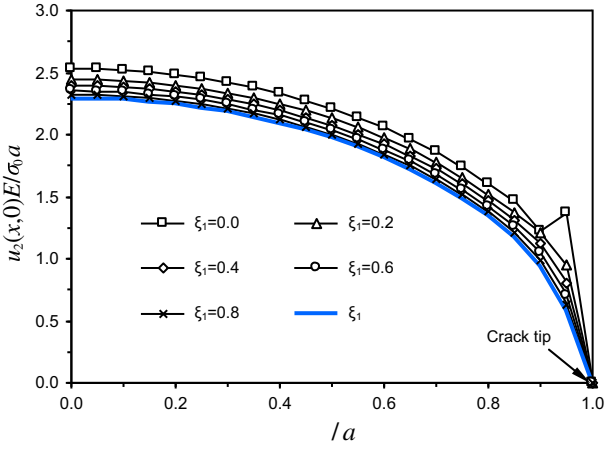

Figure 8. Opening displacement $u_2(x,0)E/\sigma_0 a$ for different portion of nonlocal elasticity while $l/a = 0.05$ and $h = b = 3a$.

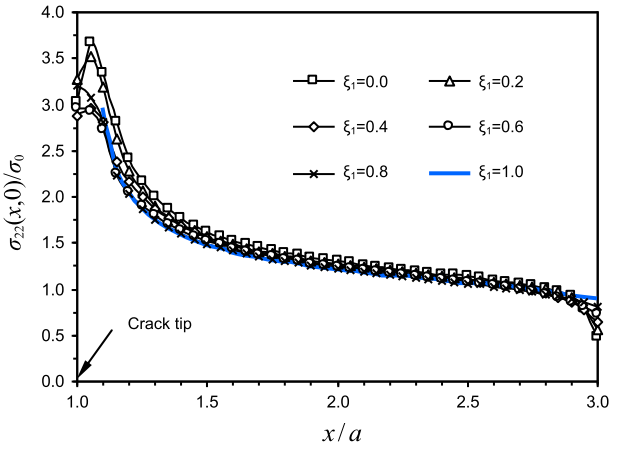

Figure 9. Normalised stress $\sigma_{22}(x,0)/\sigma_0$ for different portions of nonlocal elasticity while $l/a = 0.05$ and $h = b = 3a$.

normal stress at the crack tip $\sigma_{22}(a,0)$ increases, while the portion factor ξ_1 increases. In addition, it is observed that for pure nonlocal elasticity ($\xi_1 = 0$), the crack opening displacement is not smooth near the crack tip. Figure 8 and Figure 9 show the results of the displacement on the crack surface and stress distribution in the case of $b = h = 3a$.

Moreover, the effects of nonlocal kernel are considered. Normalised stress $\sigma_{22}(x,0)/\sigma_0$ for different nonlocal kernels $\alpha(r,l)$, while $l/a = 0.05$, $h = b = 2a$ and $h = b = 3a$ are presented in Figure 10 and Figure 11. In this case, we can estimate the degree of accuracy for approximation of stress at the crack tip by (18) and (21). In this case, the stress intensity factors are taken from the database of stress intensity factor (Aliabadi, 1996). The estimation of stresses at crack tip for two types (A and B) and

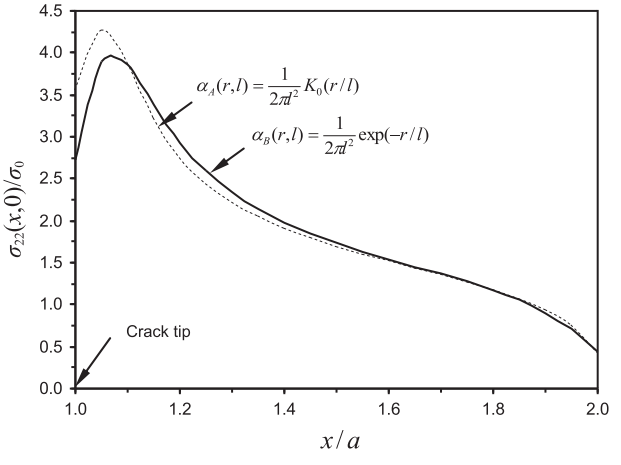

Figure 10. Normalised stress $\sigma_{22}(x,0)/\sigma_0$ for different nonlocal kernel $\alpha(r,l)$ while $l/a = 0.05$ and $h = b = 2a$.

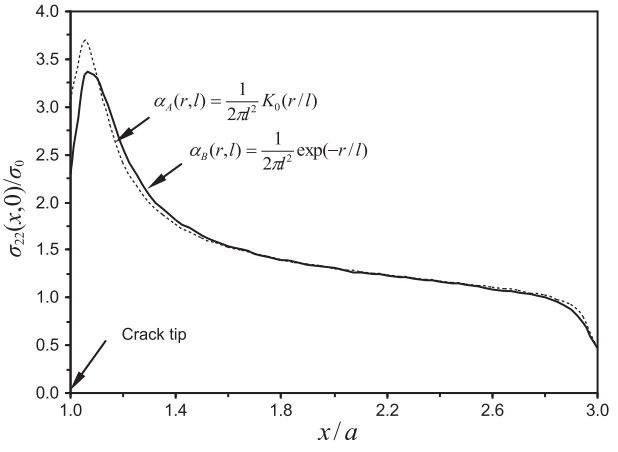

Figure 11. Normalised stress $\sigma_{22}(x,0)/\sigma_0$ for different nonlocal kernels $\alpha(r,l)$ while $l/a=0.05$ and $h=b=3a$.

Table 4. Estimations of stress at the crack tip and comparison with numerical solutions.

Type	b/a	K_I (Aliabadi, 1996)	σ_{22}/σ_0 by (18) or (21)	σ_{22}/σ_0 meshless	Error(%)
A	2.0	1.325	3.399	3.544	4.1
	3.0	1.130	2.899	3.018	3.9
B	2.0	1.325	2.847	2.730	4.3
	3.0	1.130	2.419	2.307	4.9

comparisons with meshless results are shown in Table 4. The relative errors are shown to be less than 5% for all cases.

Finally, the effects of the characteristic length l are observed with nonlocal kernel $\alpha_A(r,l)$. Normalised stress $\sigma_{22}(x,0)/\sigma_0$ for different characteristic lengths $l/a=0.05$

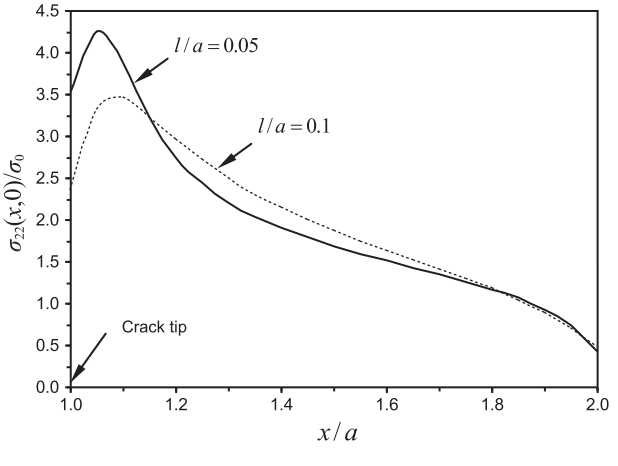

Figure 12. Normalised stress $\sigma_{22}(x,0)/\sigma_0$ for different portion l/a while $h=b=2a$.

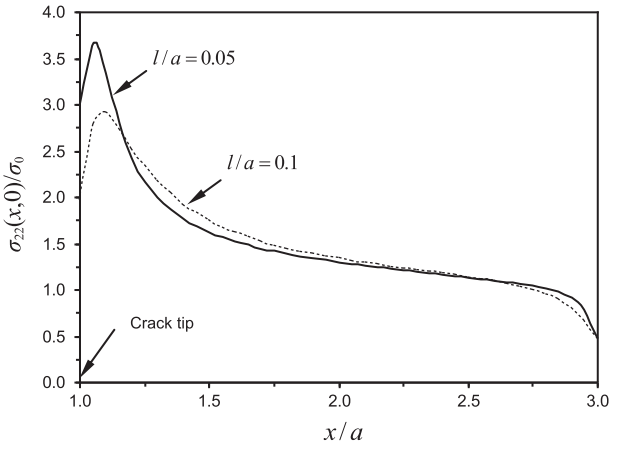

Figure 13. Normalised stress $\sigma_{22}(x,0)/\sigma_0$ for different portions l/a while $h = b = 3a$.

and 0.1, while $h = b = 2a$ and $h = b = 3a$ are presented in Figure 12 and Figure 13, respectively. It is clear that the maximum stress is located about $\xi/l = 0.5$ for each case, which agrees with the conclusion of the analytical solution.

5. Conclusions

Based on the Eringen's model, the stresses at the crack tip under tensile load and shear load at infinite of plate were approximated analytically using singular stresses of the classical theory. A weak form for a set of governing equations with a unit test function is transformed into local integral equations. Therefore, the estimation of nonlocal stresses at the crack tip can be obtained using classical mixed mode stress intensity factors. The meshless method is solved using the radial basis functions in the nonlocal elasticity fracture mechanics. To demonstrate the proposed method, a rectangular sheet with a central crack is investigated. The accuracy degree of the estimation of stresses at the crack tip is validated by the meshless method.

References

Aliabadi, M. H. (1996). *Database of stress intensity factors*. Southampton: WIT Press.

Aliabadi, M. H., Rooke, D. P., & Cartwright, D. J. (1987). An improved boundary element formulation for calculating stress intensity factors: Application to aerospace structures. *The Journal of Strain Analysis for Engineering Design, 22*, 203–207.

Altan, S. B. (1989). Existence in nonlocal elasticity. *Archive Mechanics, 41*, 25–36.

Atluri, S. N. (2004). *The Meshless Method (MLPG) for domain and BIE discretizations*. Forsyth, GA: Tech Science Press.

Bazant, Z. P. (1976). Instability, ductility and size effect in strain softening concrete. *Journal of the Engineering Mechanics Division ASCE, 12*, 331–344.

Bazant, Z. P., Belytschko, T. B., & Chang, T. P. (1984). Continuum theory for strain-softening. *Journal of Engineering Mechanics, 110*, 1666–1692.

Bazant, Z. P., & Lin, F. B. (1988). Non-local yield limit degradation. *International Journal for Numerical Methods in Engineering, 26*, 1805–1823.

Benedetti, I., & Aliabadi, M. H. (2013). A three-dimensional grain boundary formulation for microstructural modeling of polycrystalline materials. *Computational Materials Science, 67*, 249–260.

Dirgantara, T., & Aliabadi, M. H. (2000). Crack growth analysis of plates loaded by bending and tension using dual boundary element method. *International Journal of Fracture, 105*, 27–47.

Eringen, A. C. (1983). On differential equations of nonlocal elasticity and solutions of screw dislocation and surface waves. *Journal of Applied Physics, 54*, 4703–4710.

Eringen, A. C. (2002). *Nonlocal continuum field theories*. New York, NY: Springer-Verlag.

Fedelinski, P., Aliabadi, M. H., & Rooke, D. P. (1996). The Laplace transform DBEM for mixed-mode dynamic crack analysis. *Computers & Structures, 59*, 1021–1031.

Irwin, G. R. (1957). Analysis of stresses and stains near the end of a crack transverseing a plate. *ASME, Journal of Applied Mechanics, 24*, 31–364.

Lazar, M., Maugin, G. A., & Aifantis, E. C. (2006). On a theory of nonlocal elasticity of bi-Helmholtz type and some applications. International Journal of Solids and Structures*, 43*, 1404–1421.

Li, M., Hon, Y. C., Korakianitis, T., & Wen, P. H. (2013). Finite integration method for nonlocal elastic bar under static and dynamic loads. *Engineering Analysis with Boundary Elements, 37*, 842–849.

Li, L. Y., Wen, P. H., & Aliabadi, M. H. (2011). Meshfree modeling and homogenization of 3D orthogonal woven composites. *Composites Science and Technology, 71*, 1777–1788.

Mallardo, V. (2009). Integral equations and nonlocal damage theory: A numerical implementation using the BDEM. *International Journal of Fracture, 157*, 13–32.

Pisano, A. A., Sofi, A., & Fuschi, P. (2009). Nonlocal integral elasticity: 2D finite element based solutions. *International Journal of Solids and Structures, 46*, 3838–3849.

Rooke, D. P., Rayaprolu, D. B., & Aliabadi, M. H. (1992). Crack-line and edge Green's function for stress intensity factors of inclined edge crack. *Fatigue and Fracture of Engineering Materials and Structures, 15*, 441–461.

Sfantos, G., & Aliabadi, M. H. (2007). A boundary cohesive grain element formulation for modelling intergranular microfracture in polycrystalline brittle materials. *International Journal for Numerical Methods in Engineering, 69*, 1590–1626.

Sladek, J., & Sladek, V. (2006). *Advances in meshless methods*. Forsyth: Tech Science Press.

Sladek, J., Sladek, V., & Bazant, Z. P. (2003). Non-local boundary integral formulation for softening damage. *International Journal for Numerical Methods in Engineering, 57*, 103–116.

Sladek, V., Sladek, J., & Zhang, Ch (2006). Comparative study of meshless approximations in local integral equation method. *CMC: Computers Materials, & Continua, 4*, 177–188.

Wen, P. H., & Aliabadi, M. H. (2008). An improved meshless collocation method for elastostatic and elastodynamic problems. *Communications in Numerical Methods in Engineering, 24*, 635–651.

Wen, P. H., & Aliabadi, M. H. (2013). Analytical formulation of meshless local integral equation method. *Applied Mathematical Modelling, 37*, 2115–2126.

Wen, P. H., Aliabadi, M. H., Liu, Y (2008). Meshless method for crack analysis in functionally graded materials with enriched radial base functions. *CMES: Computer Modeling in Engineering & Sciences, 30*, 133–147.

Wen, P. H., Aliabadi, M. H., Rooke, D. P. (1998). Cracks in three dimensions: A dynamic dual boundary element analysis. *Computer Methods in Applied Mechanics and Engineering, 167*, 139–151.